INSTITUTE OF PHYSICS PUBLISHING NANOTECHNOLOGY

Nanotechnology **15** (2004) 907–912 PII: S0957-4484(04)76305-9

Scanning probe microscopy imaging of frequency dependent electrical transport through carbon nanotube networks in polymers

S V Kalinin[1], S Jesse[1,2], J Shin[1,2], A P Baddorf[1], M A Guillorn[1] and D B Geohegan[1]

[1] Condensed Matter Sciences Division, Oak Ridge National Laboratory, Oak Ridge, TN 37831, USA
[2] Department of Physics and Astronomy, The University of Tennessee, Knoxville, TN 37996, USA

Received 16 February 2004
Published 9 June 2004
Online at stacks.iop.org/Nano/15/907
doi:10.1088/0957-4484/15/8/006

Abstract
Frequency dependent electrical transport in the conducting networks of single walled carbon nanotubes embedded in polymers was studied by scanning impedance microscopy (SIM). SIM allows current flow in the nanotubes inside the polymer matrix at up to 100 nm below the surface to be imaged directly, providing a non-invasive approach for studying transport in these materials. The conductance of the composite is shown to be limited by a small number of bundle–bundle and bundle–contact junctions. For high frequencies, the SIM phase distribution along the networks is governed by the capacitive interaction between the nanotubes and the substrate and is in agreement with a transmission line model. For low driving frequencies the capacitive coupling to the back gate can be minimized and an approach for determining the potential distribution along the network by accounting for tip–surface capacitance variations is demonstrated. Thus, SIM provides a direct method for characterizing electrical transport through percolation networks formed by nanotube bundles in polymers or, more generally, nanorods in various matrices.

Carbon nanotube based composite materials have attracted significant attention because of their potential for unique combinations of electrical and mechanical properties. For insulating polymer matrices, nanotube networks provide percolation pathways through the polymer, rendering the composite conductive. The extremely high aspect ratio of carbon nanotubes makes them ideal for these applications since the required weight loading for percolation decreases quickly with increasing aspect ratio [1]. However, single walled carbon nanotubes (SWNTs) are mostly bundled in rope-like aggregates within polymers, and no adequate theoretical model has been developed for describing their interconnections. Optimization of the carbon nanotube–composite properties requires understanding of the nature of conductivity in the composite on the length scale of the individual bundles, including bundle–bundle and bundle–contact junctions. Recently, significant progress was achieved in the spatially resolved imaging of the transport properties of individual nanotubes using scanning probe microscopy (SPM) techniques [2–5]. However, little is known about the dc and frequency dependent transport properties of the nanotube networks. Particularly of interest is the local characterization of transport in the nanotube networks embedded within either a dielectric or electroactive polymer. The potential wide range of applications of these materials and the extreme sensitivity of transport properties of the composite to the preparation route make understanding transport on the nanoscale critical for future applications.

Here we study for the first time the conduction mechanism of nanotube networks in polymers using frequency dependent, atomic force microscopy (AFM) based transport measurements. Voltage oscillation amplitude and phase distribution in the network are measured using scanning impedance microscopy (SIM) [6, 7]. Experimental results are interpreted using a continuum transmission line model. The low frequency transport is shown to be limited to a small number of bundle–bundle junctions. It is shown that capacitive coupling between the nanotubes and the back gate governs the high frequency electrical behaviour of large networks of nanotubes, illustrating the importance of capacitive coupling for the optimal design of nanotube–polymer based thin film devices.

Nanotube–polymer composite thin films were prepared by spin casting a solution of purified laser vaporization grown SWNTs dissolved in *ortho*-dichlorobenzene (weight loadings between 10 and 100 μg g^{-1}) [8, 9] by sonication with polymethylmethacrylate (1.0–2.0 wt%) in *ortho*-dichlorobenzene as described elsewhere [10]. Solutions were spun cast onto Si/SiO_2 substrates with prepatterned gold electrode structures having spacing of either 1 or 2 μm. The resulting film thicknesses were 40–100 nm with weight loadings between 0.1 and 1.0 wt%. The surface density of the nanotubes was controlled by the casting solution concentration. Prior to SPM measurements, the geometry of the conductive network was determined by scanning electron microscopy [10]. The average dc electrical properties of individual networks were determined by I–V measurements and demonstrated high variability of transport properties between individual devices due to variations of local topology of the network.

Local frequency dependent transport properties of the nanotube network were studied using scanning impedance microscopy implemented on a commercial instrument (Digital Instruments MultiMode NS-IIIA) additionally equipped with a function generator and lock-in amplifier (DS340, SRS 830, Stanford Research Systems) as described elsewhere [6, 7]. Measurements were performed using Au coated cantilevers (spring constant $k = 1$–5 N m^{-1}, NCSC 12 Cr–Au, Micromasch). The lift height for the interleave scans was usually 100 nm. The scan rate varied from 0.5 Hz for large scans ($\sim$80 μm) to 1 Hz for smaller scans ($\sim$10 μm). The driving voltage V_{ac} in the interleave scan was 0.5 V_{pp}. Surface topography was determined in a first pass using standard intermittent contact mode detection. Electrostatic phase and amplitude data were then collected during a second pass with the tip retracing surface topography 50–100 nm above the surface. During the second pass, the tip was held at a constant bias, V_{dc}, and a lateral bias, $V_{lat} = V_{dc} + V_{ac}\cos(\omega t)$, is applied across the sample through the micropatterned electrodes. To observe the lateral transport through the network, one of the electrodes was biased. Alternatively, both electrodes can be biased simultaneously to establish uniform potential across the network. The lateral bias induces an oscillation in surface potential

$$V_{surf} = V_s + V_{ac}(x)\cos(\omega t + \varphi(x)) \qquad (1)$$

where $\varphi(x)$ and $V_{ac}(x)$ are the position dependent phase shift and voltage oscillation amplitude and V_s is the dc surface potential. Oscillation of the surface potential results in a periodic force on the cantilever resulting in mechanical deflection. The amplitude of the cantilever deflection is proportional to the electrostatic force, while the phase has a position independent lag between voltage oscillations on the surface and mechanical vibrations of the cantilever due to the inertia of the probe. The variation of the phase (SIM phase image) provides the true voltage phase variation along the network since the phase lag is constant along the surface. This phase and amplitude information allows local capacitive and resistive behaviour to be determined and correlated with individual microstructural features [7, 11].

Surface topography and SIM amplitude images of the polymer-embedded nanotube network are shown in figure 1. The surface topography images exhibit height variations at the locations of the nanotubes; however, the topology of the network cannot be established from topographic data due to the large number of topographic features associated with substrate roughness and partial dewetting of the polymer. The SIM amplitude images clearly illustrate the potential distribution along the network. It is noteworthy that SIM accesses the transport along the nanotubes *inside* the polymer matrix at a 0–100 nm depth, and provides an approach for local non-invasive transport measurements of thin film composite materials. In particular, the fact that observation of a biased nanotube in the vicinity of the contact requires an electrical connection between the two suggests that the nanotube is located on the bottom of $\sim$100 nm thick film.

In the top electrode biased configuration of figure 1(c), the potential attains its maximal value on the biased electrode and is virtually uniform along the network. Reversing the bias direction changes the potential distribution throughout the network as is illustrated in figure 1(d). The potential distribution in the network is represented in schematic form in figures 1(e), (f). Direct comparison of these two images illustrates that in the top biased configuration only a part of the total conductive network is biased and that a significant potential drop occurs at the bottom electrode contact. For the bottom biased electrode configuration, significant potential drops occur at the top electrode. In addition, significant potential drops appear at the nanotube junctions indicated in figure 1(f). Thus, direct comparisons of the images allow unambiguous determination of both the conducting pathways and the key junctions responsible for transport in the nanotube network.

Further information on frequency dependent transport behaviour of the nanotube networks can be obtained from the combined SIM phase and amplitude images. Illustrated in figure 2 are large scale SIM amplitude and phase images in the top, bottom and dual biased electrode configurations. Note that the potential amplitude decays with the separation from the biased electrodes even in the dual electrode configuration (figure 2(a)). This is unexpected, since in the absence of current sinks (grounded contacts) the nanotube network well above the percolation threshold is expected to be uniformly biased. At the same time, SIM phase images clearly exhibit significant phase variations along the network. While the phase shift at the electrodes is zero as chosen by the phase offset of the lock-in amplifier, there is a significant ($\sim$10°–20°) phase change detected between the electrode and the nanotubes. The phase

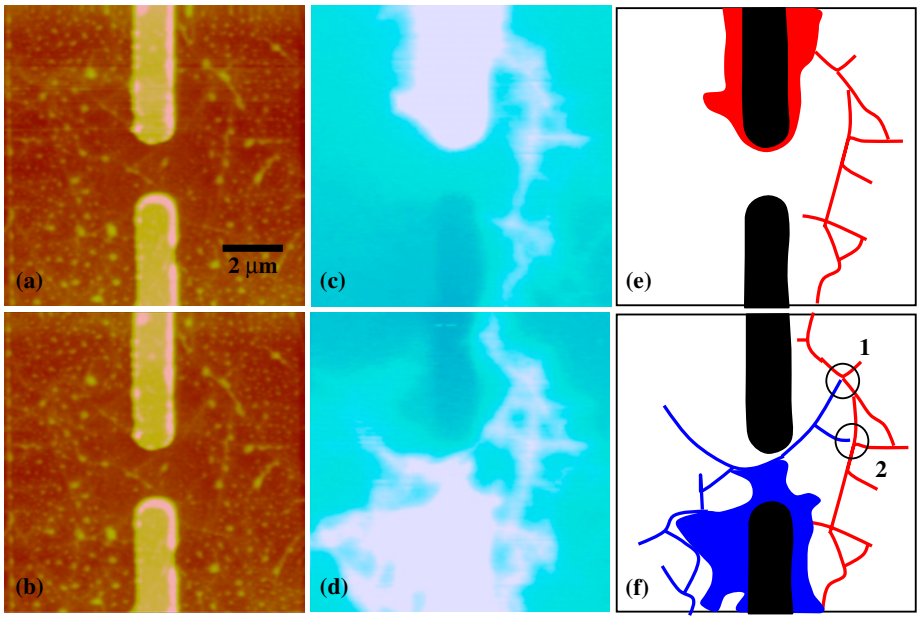

Figure 1. Surface topography ((a), (b)) and SIM amplitude images ((c), (d)) for top ((a), (c)) and bottom ((b), (d)) biased electrode configurations. The schematic potential distribution in the top (e) and bottom (f) biased networks. Shown in red is the segment of the network biased through either contact, in blue the part of the network biased through the bottom contact only. 1 and 2 indicate the location of highly resistive junctions within the network. Direct comparison of the images under different bias conditions allows unambiguous determination of the transport topology of the network.

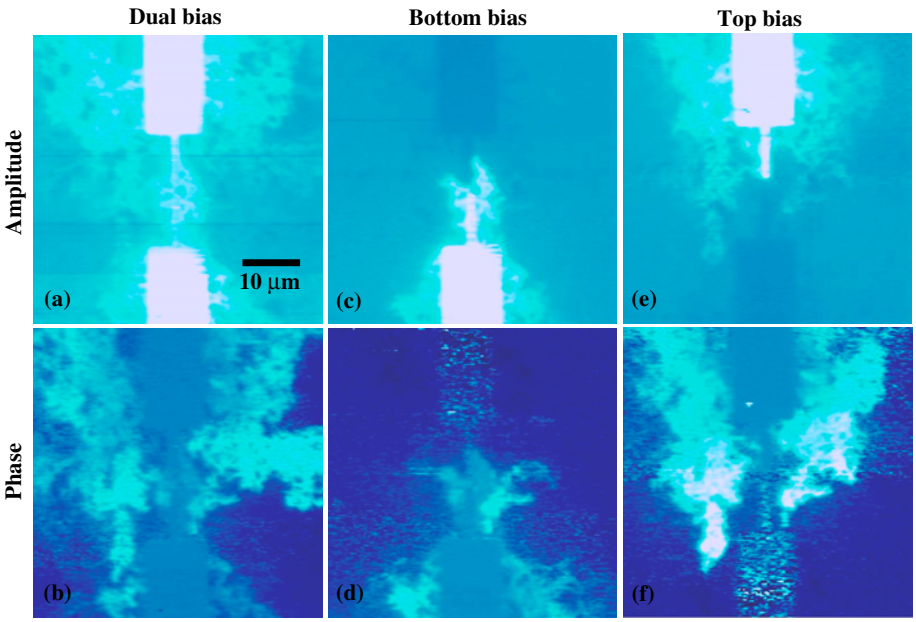

Figure 2. SIM amplitude and phase images in the dual, bottom and top biased electrode configurations. SIM amplitude ((a), (c), (e)) and phase ((b), (d), (f)) images in the dual ((a), (b)), bottom ((c), (d)) and top ((e), (f)) biased configurations. The scale of the phase images is 60°.

distribution along the network is non-uniform and generally increases with the separation from the contact, as clearly seen in figure 2(f).

To account for this unusual behaviour, we consider the capacitive coupling between the network and grounded back gate electrode. Indeed, for the dc biased network in the absence of current sinks the dc potential is expected to be uniform, while in the ac case capacitive coupling between nanotube and back gate provides a channel for current. To quantitatively analyse this frequency dependent behaviour, we use a transmission line model (figure 3) [12]:

$$\frac{\mathrm{d}^2 V_{\mathrm{ac}}(x)}{\mathrm{d}x^2} = \mathrm{i}\omega RC V_{\mathrm{ac}}(x) \tag{2}$$

where $V_{\mathrm{ac}}(x)$ is the position dependent local ac bias amplitude, R is the resistivity of the nanotube, C is the specific nanotube–substrate capacitance and ω is the signal frequency. The boundary conditions for an infinitely long nanotube biased on

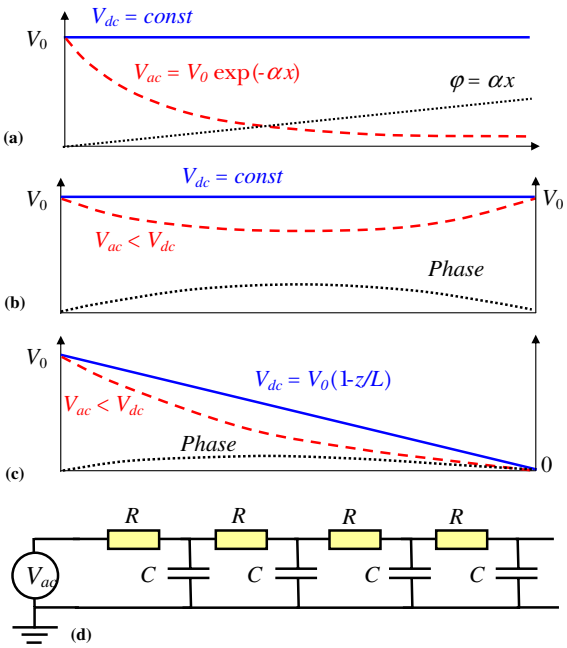

Figure 3. Predicted potential, amplitude and phase distributions across conductive segments within a network for various boundary conditions. dc potential (solid line) and ac potential amplitude (dashed line) and phase (dotted line) distributed along an individual nanotube for (a) the infinite nanotube, (b) the dual electrode biased nanotube and (c) the single electrode biased nanotube. (d) The equivalent circuit of a transmission line capacitively coupled to the ground.

one end at the electrode are $V(0) = V_{ac}$ and $V(\infty) = 0$. The potential distribution along the nanotube is then given by $V_{ac}(x) = V_{ac}\exp[-x\sqrt{\mathrm{i}R\omega C}]$ or

$$V_{ac}(x) = V_{ac}\exp(-\alpha x)(\cos\alpha x + \mathrm{i}\sin\alpha x) \qquad (3)$$

where $\alpha = \sqrt{R\omega C/2}$, as illustrated in figure 3. SIM experimentally measures the force amplitude proportional to $V_{ac}(x)$, and the phase, $\varphi(x)$, of the voltage oscillations on the surface. From equation (3) these are $V_{ac}(x) = V_{ac}\exp(-\alpha x)$ and $\varphi(x) = \alpha x$. This implies that the voltage amplitude along the nanotube should decrease exponentially with distance at the rate determined by the decay constant, α, while the phase angle should change linearly along the nanotube. For a nanotube network, in which the resistance is dominated by junctions within and between the bundles, the measured phase shifts and amplitudes are expected to be uniform within conductive segments and change abruptly at the high resistance junctions.

A similar analysis can be performed for the case when a nanotube is in contact with two electrodes at equal bias. In the dc case, the potential is uniform along the entire network. However, for frequency dependent transport, capacitive coupling between the nanotubes and the substrate leads to potential drops along the nanotubes. In this case, the potential distribution along the nanotube can be found by solving equation (2) with the boundary conditions $V(0) = V_0$ and $\mathrm{d}V(L/2)/\mathrm{d}x = 0$ in the centre of the nanotube as

$$V_t(x) = V_0\frac{\exp((L-x)\sqrt{\mathrm{i}\omega CR}) + \exp(x\sqrt{\mathrm{i}\omega CR})}{1+\exp(L\sqrt{\mathrm{i}\omega CR})}. \qquad (4)$$

For small decay constants $\alpha L \ll 1$ the potential distribution along the nanotube is

$$V_t(x) = V_0\left\{1 - \frac{\mathrm{i}}{2}a^2(L-x)x - \frac{1}{24}a^4(L^3 - 2Lx^2 + x^3)x\right\}. \qquad (5)$$

For a laterally biased nanotube between two electrodes with $V(0) = V_0$ and $V(L) = 0$, the corresponding solution is

$$V_t(x) = V_0\frac{\exp((2L-x)\sqrt{\mathrm{i}\omega CR}) - \exp(x\sqrt{\mathrm{i}\omega CR})}{-1+\exp(2L\sqrt{\mathrm{i}\omega CR})} \qquad (6)$$

and for small decay constants $\alpha L \ll 1$,

$$V_t(x) = V_0\left(1 - \frac{x}{L}\right) - \mathrm{i}V_0 x\frac{(2L^2 - 3Lx + x^2)a^2}{6L}. \qquad (7)$$

Hence, for small decay constants corresponding to highly conductive nanotubes and low frequencies, $\omega \ll 1/RCL^2$, the potential distribution is virtually uniform along a nanotube biased on both ends. For small α, the phase signal provides a convenient and better measure of the decay constant than the amplitude. This is because amplitude is directly proportional to the tip–tube capacitance and hence nanotube diameter, whereas phase is independent of the tip–tube capacitance. Thus, phase measurements provide a reliable characteristic of ac bias distribution and transport properties of a network.

To establish the parameters of the polymer-embedded nanotube network, the macroscopic transport properties were studied by means of two-probe transport measurements between the electrodes. The resistances measured for various 1 μm sections of our nanotube networks were determined to be in the range 10 MΩ–10 GΩ, from which the effective resistivities can be estimated to be in the range $R/L \sim 10^{13}$–10^{16} Ω m^{-1}. The nanotube–substrate capacitance is modelled by the cylindrical capacitor model, $C = L2\pi\varepsilon\varepsilon_0/\ln(d/R)$, where R is bundle radius, d is the oxide thickness, L is the nanotube length and ε is the dielectric constant of the oxide. For $R = 4$ nm and $d = 500$ nm, the effective capacitance can be estimated as $C/L = 4.61 \times 10^{-11}$ F m^{-1}. From these estimates, the decay constant along the network is $\alpha = (0.48\text{–}15.2) \times 10^3\sqrt{\omega}$ m^{-1}, where ω is in kHz. Typical frequencies of the order of ~100 kHz yield characteristic decay lengths, $l = 1/\alpha$, from $l \sim 200$ to ~6 μm depending on the nanotube resistance. Hence, for a poorly conductive nanotube network, the ac potential is expected to be confined to within a few microns of the electrode. Conversely, applying bias to a well conducting network effectively biases the network over hundreds of microns.

This predicted transport behaviour is in qualitative agreement with experimental observations in figure 2. To quantify this behaviour, the frequency dependence of the average phase lag at 20 μm separation from the contact was measured and plotted in figure 4. For low frequencies ($\omega <$ 50 kHz), this behaviour clearly follows a $\varphi \sim \sqrt{\omega}$ dependence in agreement with equation (5). From the linear part of the plot, the average RC product of the nanotube network can be estimated as 3.23×10^4 s m^{-2}. The decay length at 100 kHz is then $\alpha^{-1} = 25$ μm which is in a good agreement with the observed potential decay length in figures 3(a), (c) and (e). The phase shift saturates at high frequencies which can be ascribed

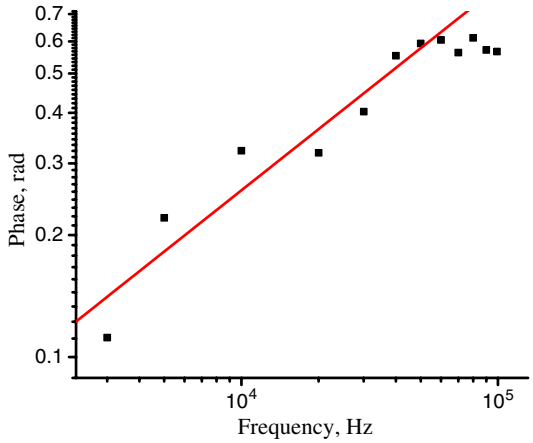

Figure 4. The frequency dependence of the measured SIM phase at fixed separation from the contact for the network shown in figure 2. The phase shift behaviour follows a $\varphi \sim \sqrt{\omega}$ dependence as predicted by equation (5).

to the dominant contribution of the back gate at large distances from the contact.

Finally, SIM is used to determine the true potential distribution across the network and nanotube–contact junction. The measured SIM amplitude signal is proportional to the product of the local ac potential, $V_{ac}(x)$, and the position dependent tip–surface capacitance gradient, $F_{1\omega}^{cap}(x) \sim C'_{nt} V_{ac}(x)$. Thus, the potential drop at the biased electrode–nanotube interface cannot be determined directly from these data because of the large difference between the tip–tube and tip–surface capacitances. To account for the local variations in the tip–surface capacitance, we collect SIM data for a uniformly biased network, for which $V_{ac}(x) = \text{constant}$. This corresponds to the dual biased electrode configuration in the low frequency limit, in which the potential distribution along the nanotube network is not affected by the capacitive coupling with the back gate. Experimentally this corresponds to the uniform or weakly changing phase contrast along the investigated part of the network. In this case, the potential distribution in the network can be obtained from SIM amplitude data by dividing a single electrode biased image (for instance, figure 2(c) or 2(e)) by a dual electrode biased image (figure 2(a)) and then renormalizing the image by the value of the applied bias, V_{ac}. This normalization procedure is illustrated in figure 5. Note that the measured SIM amplitude in figure 5(a) changes strongly between contacts and the nanotube network due to the large difference between tip–tube and tip–contact capacitances. On the normalized image, figure 5(b), the potential is constant between the contact and the tube network and within the network. Interestingly, the potential drop occurs only at the interface between the nanotubes and the top contact. The normalized potential distribution for the biased top contact is shown in figure 5(c). In this case a large part of the nanotube network is grounded, indicating a high resistance of the top contact and the presence of resistive tube–tube junctions.

In summary, frequency dependent transport through carbon nanotube networks embedded in polymers was studied using SIM. Transport behaviour was observed even for the nanotubes at ∼100 nm depth below the surface, illustrating the applicability of SIM for non-invasive transport imaging in nanocomposite materials. The voltage oscillation amplitude and phase distribution in the network were measured and quantified using a simple transmission line model. At low frequencies, transport is shown to be dominated by a small number of bundle–bundle junctions. At high frequencies, the transport behaviour of the networks is governed by the capacitive coupling between the nanotubes and the back gate resulting in potential decay along the network at large separations from the contacts. The decay length was found to depend significantly on the network resistance and can range from ∼10 μm for poorly conductive networks to ∼10 cm for conductive networks of nanotubes. For low frequencies, the potential distribution along the network can be derived by division of a single electrode biased image by a dual electrode biased image which accounts for any variations in tip–sample capacitance. These techniques can be extended to the characterizing and understanding of frequency dependent transport in percolation networks formed by nanotube bundles in other polymers as well as, and more generally, by nanorods and nanowires in various matrices.

Acknowledgments

This research was sponsored in part by the Eugene P Wigner Fellowship at the Oak Ridge National Laboratory, managed

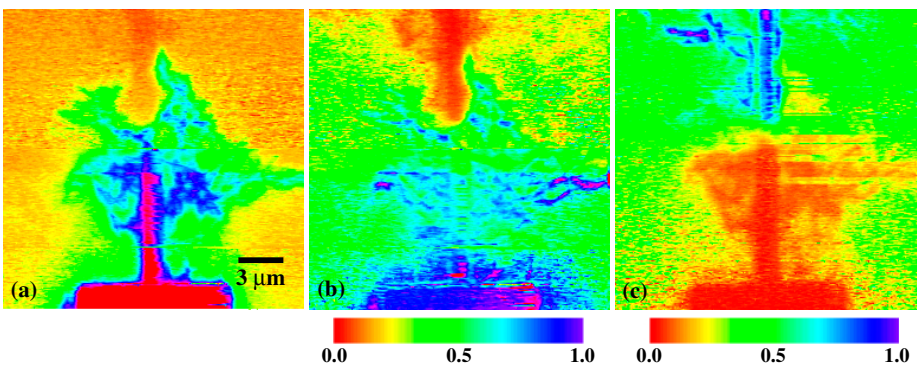

Figure 5. (a) A SIM amplitude image in the bottom biased configuration. Note the significant amplitude change at the nanotube–electrode contact due to the capacitance differences. (b) A SIM voltage image generated by dividing figure 2(c) by 2(a) and normalizing by the V_{ac} value, thus providing the potential distribution along the network. Note the absence of a potential drop at the tube–contact interface. (c) A normalized SIM image in the top biased configuration (figure 2(e)). The maximum bias corresponds to 0.5 V_{pp}.

by UT-Battelle, LLC, for the US Department of Energy under Contract DE-AC05-00OR22725 (SVK). Additional funding was provided by the Laboratory Directed and Development Program at ORNL in conjunction with NASA-Langley Research Center (DBG) and Laboratory SEED funding (SVK).

References

[1] Balberg I and Binenbaum N 1983 *Phys. Rev.* B **28** 3799
[2] Bachtold A, Fuhrer M S, Plyasunov S, Forero M, Anderson E H, Zettl A and McEuen P L 2000 *Phys. Rev. Lett.* **84** 6082
[3] Freitag M, Johnson A T, Kalinin S V and Bonnell D A 2002 *Phys. Rev. Lett.* **89** 216801
[4] Tans S J and Dekker C 2000 *Nature* **404** 834
[5] Freitag M, Radosavljevic M, Clauss W and Johnson A T 2000 *Phys. Rev.* B **62** R2307
[6] Kalinin S V and Bonnell D A 2001 *Appl. Phys. Lett.* **78** 1306
[7] Kalinin S V and Bonnell D A 2002 *J. Appl. Phys.* **91** 832
[8] Geohegan D B, Schittenhelm H, Fan X, Pennycook S J, Puretzky A A, Guillorn M A, Blom D A and Joy D C 2001 *Appl. Phys. Lett.* **78** 3307
[9] Britt P F, Viswanathan S, Ivanov I N, Puretzky A A, Lance M J and Geohegan D B 2003 *American Physical Society March Mtg (Austin, TX, March 2003)*
[10] Jesse S, Guillorn M A, Ivanov I N, Puretsky A A, Howe J Y, Britt P F and Geohegan D B 2004 to be submitted
[11] Kalinin S V, Suchomel M R, Davies P K and Bonnell D A 2002 *J. Am. Ceram. Soc.* **85** 3011
[12] Lebedev N N, Skal'skaya I P and Uflyand Ya S 1966 *Problems in Mathematical Physics* (Oxford: Pergamon)